Optimal Power Flow Through Variable Frequency Transformer Using Different Optimization Techniques

Aabid Hussain Sheikh* and Farhad Ilahi Bakhsh

Department of Electrical Engineering, NIT Srinagar, Hazratbal – 190006, Srinagar (J&K), India
E-mail: aabidqoya91@gmail.com
**Corresponding Author*

Received 03 November 2021; Accepted 02 February 2022;
Publication 22 April 2022

Abstract

For synchronous and asynchronous connectivity of separate power grids, phase shifting transformers (PST), the high-voltage-direct-current (HVDC) converters and variable-frequency-transformer (VFT) are viable options. Natural damping and high overloading capabilities are inherent in the VFT, which is critical for power grid reliability and stability. This article reports the optimal power flow across a power system involving the implementation of several meta-heuristic optimization techniques based control strategy. Several optimization techniques are applied to optimize the gains of proportional-integral-derivative (PID) controller which aids in regulating the system dynamic response. The firefly algorithm based PID controller performs better in contrast to other optimization techniques in improving the system dynamics. The DC motor accustomed with PID controller provides the required torque necessary for power transfer between two connected grids. Sensitivity analysis is exhibited to inspect the strength of developed power system against deviations in certain system parameters. A separate study is done for the asynchronous operation of VFT based power system using firefly

Distributed Generation & Alternative Energy Journal, Vol. 37_4, 1129–1158.
doi: 10.13052/dgaej2156-3306.37410

algorithm with different DC motor torque. To validate the effect of VFT over HVDC total harmonic distortion analysis has been carried out to check for the harmonic content in the rotor and stator current of VFT.

Keywords: Variable frequency transformer (VFT), high-voltage-direct-current (HVDC), sensitivity analysis (SA), firefly algorithm (FA).

1 Introduction

The classical synchronous interconnection between two power grids is realized by using PST and the asynchronous interconnection is accomplished using back-to-back (B2B) HVDC link. Conversely, achieving synchronous power system interconnection using PST in the modern power systems is difficult when one or both power grids experience a slight change in frequency. Moreover, the PST provides slow and step-wise change causing deterioration to the contacts of tap changer [1]. To achieve the power interchange among connected asynchronous power grids, a B2B HVDC link is employed extensively. A line commuted converter (LCC) established HVDC tie endures from the drawbacks of deficit inertia for natural damping, lesser thermal time constant leading to short over load capability and ample reactive power requirement. Whereas, the reactive power requirement can be controlled by voltage source converter (VSC) established HVDC tie unlike LCC established HVDC tie but the introduction of harmonics, frequency response and contribution of inertia are still the objections faced by HVDC technologies [2]. Consequently, the incorporation of VFT between power grids for power transfer can address the above mentioned challenges.

VFT comprises of three core components: (1) Dc Drive motor (2) Rotary transformer (3) Collector bus. The rotary transformer is basically a conventional induction machine having wound rotor as doubly-fed (WRIM) and loaded with three-phase winding on both stator and rotor. On the upper side of the rotary transformer are the three-phase collectors. The rotor winding and the collector rings are connected through a three-phase bus. The collector is made using traditional method that uses carbon brushes on copper slip rings. All these components are coupled on a same shaft [3]. Figure 1 depicts the single line diagram of VFT incorporated between two power grids. The stator of VFT is electrically linked with power Grid #1 and the rotor is linked with power Grid #2. The air gap between the three phase stator and rotor windings provides the required magnetic coupling which is necessary for power interchange in between connected power grids. Power transfer between

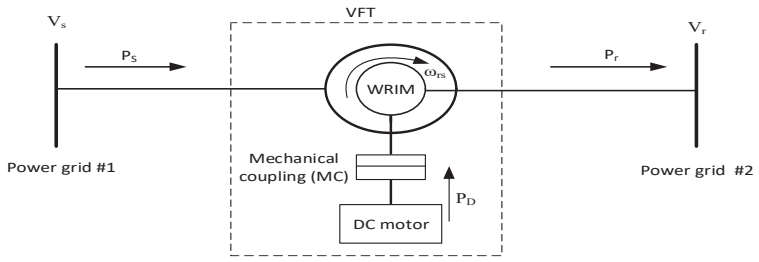

Figure 1 System outline of VFT.

power grids occurs through a phase angle shift which is created by the torque provided by the dc motor, coupled to the rotor of VFT. The amount as well as the direction of active power across VFT depends on the phase angle shift and other VFT parameters [3].

1.1 Related Works

The concept of VFT is introduced by authors in [3] along with its electromagnetic and mechanical design. The necessary features of dc motor required for the generation of torque in VFT is reported in [4]. In the work presented in [4], a 20 Pole, 48/93 rpm, 2796 KW, 750V VFT installation is done with a dc motor. The work in [5] describes the use of VFT to transmit power across synchronous and asynchronous power grids. The performance comparison of VFT and B2B HVDC tie for power transfer to a weak AC network is discussed in [6] and it reveals that VFT provides better natural damping capability and faster initial transient recovery as compared to other counterparts. The role of VFT for the prevention of fault propagation into adjoining area's is explained in [7]. The simulation findings in [7] clearly demonstrate that the VFT successfully reduces power oscillations. and thus helps in preventing the fault from spreading to other areas. A control strategy is developed in for VFT to achieve the low voltage ride through capability. The control scheme in employs a dynamic series braking resistor to limit the fault spread across VFT. Another control strategy based on series compensation technique is developed in [8] to restrict the VFT against asymmetrical grid faults. Application of VFT in wind energy conversion systems (WECS) is discussed in [9]. The modelling results in [9] clearly depict that VFT is capable of transferring power from WECS to power grid at different PMSG speeds with the production of negligible harmonics. Also, the application of VFT to feed an isolated load is carried out in [10] and it is revealed that when proposed system is compared to a typical conventional system,

overall harmonic distortion of output voltage and current of proposed system is minimal. Another novel control strategy is presented in [11] to reduce the disturbances using VFT in doubly fed induction generator based WECS. A detailed configuration of power transfer control through VFT with separated active and reactive power is presented in [2]. The work imposes series voltage compensation to achieve decoupled and bi-directional power flow. Another work presented in [12] implements VFT to suppress power fluctuations in wind turbine using PID controller. The PID controller gains in [12] is optimized using particle swarm optimization.

To regulate load frequency, the work presented in [13] implements grey wolf optimization (GWO) in an interconnected power system. To diminish the inter-area oscillations in a power system, a stabilizer is used in [14], and moreover the controller gains are adjusted capitalizing GWO. To unravel the optimal power flow problem in power system, water evaporation optimization (WEO) is implemented in [15]. To determine the efficiency of WEO various IEEE bus systems are tested in [15]. Another similar work presented in [16] discusses the optimal power flow problem using WEO and its competitiveness in addressing a variety of objectives is demonstrated by a comparison study with other well-established methodologies. In [17], the firefly algorithm (FA) is used to improve the hybrid fuzzy PID controller gains in a multi-area system for load frequency management. To test the effectiveness of the suggested method in [17], time domain simulations are run with various contractual situations and the obtained outcomes are compared. The work demonstrated in [18] plans out a method for minimizing the ohmic power loss of an overall network by improving control variables like series injected voltage magnitude by unified power flow controller (UPFC) and its phase angle, UPFC location and transformer taps using a bio-inspired optimization technique called as the firefly algorithm (FA). The work presented in [19] implements flywheel energy storage system and VFT to mitigate the power frequency oscillations in wind integrated two area power system. To enhance load frequency control in an interconnected power system, VFT is combined with a fuzzy-based super capacitor energy storage device [20].

Since, none of the optimization techniques mentioned in the literature have been implemented on VFT based power system. Therefore, this work manages to implement the same to optimize the PID controller gains and to test the effectiveness of the PID controller gains, sensitivity analysis has been performed. Moreover, total harmonic distortion (THD) analysis has been carried out to check against the harmonic content in the rotor and stator current of VFT.

This paper is arranged in 7 sections. Section 2 presents the motivation, contribution and objectives of the present work. Section 3 provides the general theory of operation of VFT along with the related mathematical equations. Section 4 discusses the MATLAB model of power system in consideration. Section 5 explains the basic operation of the optimization techniques employed in the current work. Section 6 presents the results and discussions along with the sensitivity analysis, asynchronous operation and THD analysis of VFT. Finally Section 7 draws the conclusion.

2 Motivation

Computational problems may occur in today's reality while trying to identify a globally optimum solution from an enormous solution space. As a result, heuristic optimization algorithms that can discover the candidate solution from a huge solution space have been proposed. Various meta-heuristic optimization techniques have recently been presented to handle real-time, complicated and non-linear issues. Optimization techniques are more popular than conventional techniques due to local optima avoidance, derivative free mechanism, flexibility and simplicity. The present work aims at evaluating the dynamic performance regulation of VFT based power system incorporated with realistic behavior in the form of non-linearities and complexity through real-time simulations. Hence, optimization techniques are applied in order to take care of the system realistic behavior.

2.1 Contribution and Objectives of Present Work

A VFT based power system is analyzed for optimal power flow between two connected power grids in both synchronous and asynchronous modes. The power interchange is realized by means of industrially applied PID controller, the gains of which are optimized using several meta-heuristic techniques available in literature. The robustness of PID controller gains is verified using sensitivity analysis by subjecting the nominal system through different parameter variations.

Objectives of Present Work

Based on the above discussions the objectives are:

1. To develop and model VFT based power system for power transfer between two connected power grids.

2. To compare the system performance in presence of PID controller using different meta-heuristic optimization techniques.
3. To evaluate the optimum meta-heuristic optimization technique for desired performance of the developed power system.
4. To check the robustness of optimized PID controller gains for alterations in system parameters from their nominal values.
5. To investigate the operation of VFT based power system under asynchronous condition.
6. To analyze the harmonic content in stator and rotor current of VFT under synchronous and asynchronous condition using THD analysis.

3 Theory of Operation of VFT

In case of VFT, while applying the torque on the shaft, the phase angle between stator and rotor windings gets continuously modified. Thus, power gets continuously varied. Therefore, the equation for active power transfer through VFT is given by Equations (1) and (2). The circuit diagram of power system network with VFT incorporated is shown in Figure 2 and phasor diagram representation of the VFT is presented in Figure 3.

$$P_{VFT} = \frac{V_1 V_2}{X_l + X_{VFT}} \sin(\theta_1 - (\theta_2 + \theta_{2o})) = \frac{V_1 V_2}{X_{12}} \sin(\theta_1 - (\theta_2 + \theta_{2o})) \tag{1}$$

$$P_{VFT} = \frac{V_1 V_2}{X_{12}} \sin(\theta_{net}) \tag{2}$$

$\theta_{net} = \theta_1 - (\theta_2 + \theta_{2o})$
$\mathrm{P_{VFT}}$ = Power flow through VFT.
$\mathrm{V_1}$ = Magnitude of voltage on stator.
$\mathrm{V_2}$ = Magnitude of voltage on rotor.
X_{12} = Net stator to rotor reactance.

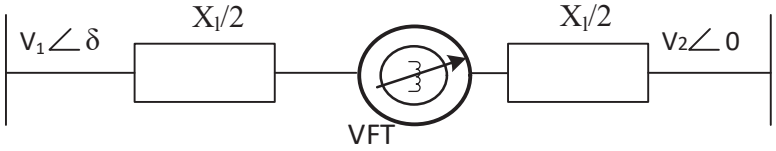

Figure 2 Circuit diagram of VFT.

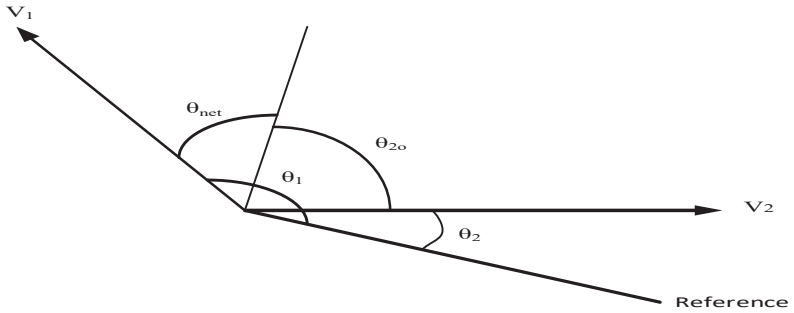

Figure 3 Phasor relationship of voltages in VFT based power system.

$\theta_1 =$ Stator voltage phase angle w.r.t reference phasor.
$\theta_2 =$ Rotor voltage phase angle w.r.t reference phasor.
$\theta_{2o} =$ Net stator to rotor phase angle.

The maximum possible power transfer occurs at $\theta_{net} = 90^\circ$ in either direction

$$P_{VFT} = \frac{V_1 V_2}{X_{12}}; \quad \text{at } \theta_{net} = \theta_1 - (\theta_2 + \theta_{2o}) = 90^\circ \tag{3}$$

But for stable operation of the VFT, angle θ_{net} must be less than 90°. The time integral of AC voltage frequencies gives their respective angles, while the integral of rotor speed over time gives the angle of rotor and is given in Equation (4).

$$P_{VFT} = P_{\max} \left[\int (\omega_1(t) - \omega_2(t))dt - \int \omega_{2o}(t)dt \right] \tag{4}$$

Where,

$\omega_1 =$ Time dependent voltage frequency at stator terminals.
$\omega_2 =$ Time dependent voltage frequency at rotor terminals.
$\omega_{2o} =$ Time dependent rotary transformer rotor speed.

4 Power System Under Investigation

The system under investigation is modelled under MATLAB/SIMULINK platform as shown in Figure 4. A 400 V three phase source is used to simulate both the grids. For synchronous operation both the grids are kept at 50 Hz while for an asynchronous operation 60 Hz and 50 Hz frequencies

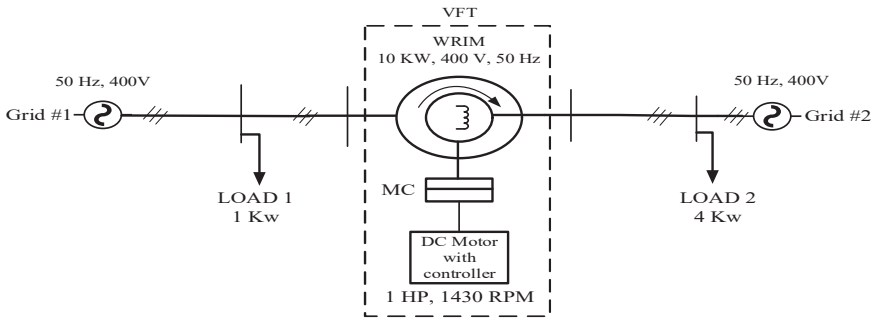

Figure 4 Schematic diagram of developed power system.

are employed for Grid #1 and Grid #2 respectively. The WRIM stator is linked with Grid #1 while as the rotor of WRIM is linked with Grid #2. The WRIM which is basically a rotary transformer is rated at 10 Kw, 50 Hz, 400 V and 1430 RPM. The output torque of dc shunt motor rated at 240 V, 1 HP, 1430 RPM is applied to the rotor of WRIM to simulate the VFT. A load of 1 Kw is connected to Grid #1 while as a load of 4 Kw is connected to Grid #2. A PID controller is accustomed with the dc shunt motor to control the torque which eventually controls the power transfer between two grids. The developed model is used to assess the performance of the power system in consideration.

5 Optimization Techniques Applied

For the desired performance evaluation of the developed power system, some recent optimization techniques are considered. These are discussed below;

5.1 Water Evaporation Optimization

A. Kaveh et al. introduced water evaporation optimization (WEO) [21] and it implements molecular dynamics to examine water particles evaporating from solid surfaces of varying wettability. Wettability is a criterion of liquid particle's capacity to attach to solid surfaces and is denoted by the interaction between solid phases and fluid. By changing the charge (q), the wettability can be restrained. The mobility of water depends on q and stretches smoothly to the value of $q = 0.4e$. As the value of q drops below 0.4e, the water droplet shrinks considerably and becomes immobile. The search space is represented by the solid surface with different wettability whereas, individuals are represented by water particles in WEO. As the algorithm progresses,

changes in water accumulation over the surface occurs due to the variations in surface wettability and these variations are interpreted as changes in the values of objective function. Those individuals who achieve their maximum around q = 0.4e have a chance to update themselves and this is represented by evaporation flux. This helps the WEO to achieve simplified algorithm structure and good convergence rate. The individuals in WEO are updated using Equation (5).

$$E_f(q) = \exp\left(\frac{-E_{cs}}{K_B T_{room}}\right); \quad q \geq 0.4e \tag{5}$$

Where, $E_f(q)$ denotes evaporation flux, E_{cs} denotes the surface contact energy, T_{room} denotes room temperature and K_B denotes Boltzmann constant.

For half number of evaluations monolayer evaporation (ME) probability given in Equation (6) is used to update the individuals of WEO. The global search competence of WEO is represented in this first phase.

$$\begin{aligned} ME_{ij}^k &= 1 \quad for\ rand_{ij} \langle \exp(E_{cs}(i)^k) \\ ME_{ij}^k &= 0 \quad for\ rand_{ij} \geq \exp(E_{cs}(i)^k) \end{aligned} \tag{6}$$

$$\begin{aligned} DE_{ij}^k &= 1 \quad for\ rand_{ij} \langle \exp(Ef(\phi(i))^k) \\ DE_{ij}^k &= 0 \quad for\ rand_{ij} \geq \exp(Ef(\phi(i))^k) \end{aligned} \tag{7}$$

Where,

$$\phi(i)^k = \frac{(\phi_{high} - \phi_{low}) \times (OF_i^k - low(OF))}{high(OF) - low(OF)} + \phi_{low} \tag{8}$$

$ME_{ij}^k$and DE_{ij}^k (given in Equation (7)) represents the chances at *k*th iteration to update the *j*th variable of *i*th water particle in ME and DE probability and ϕrepresents the contact angle vector.

Droplet evaluation probability given in Equation (9) is used to update the individuals in the second phase.

$$E_f(\phi) = E_0 P_g(\phi);\ q < 0.4e \tag{9}$$

Where, $E_f(\phi)$ is evaporation flux, E_0 is a constant having a value of $1.24\ ns^{-1}$ and $P_g(\phi)$ is the ratio of condensed water particles and surface water particles. The flowchart of WEO is given in Figure 5.

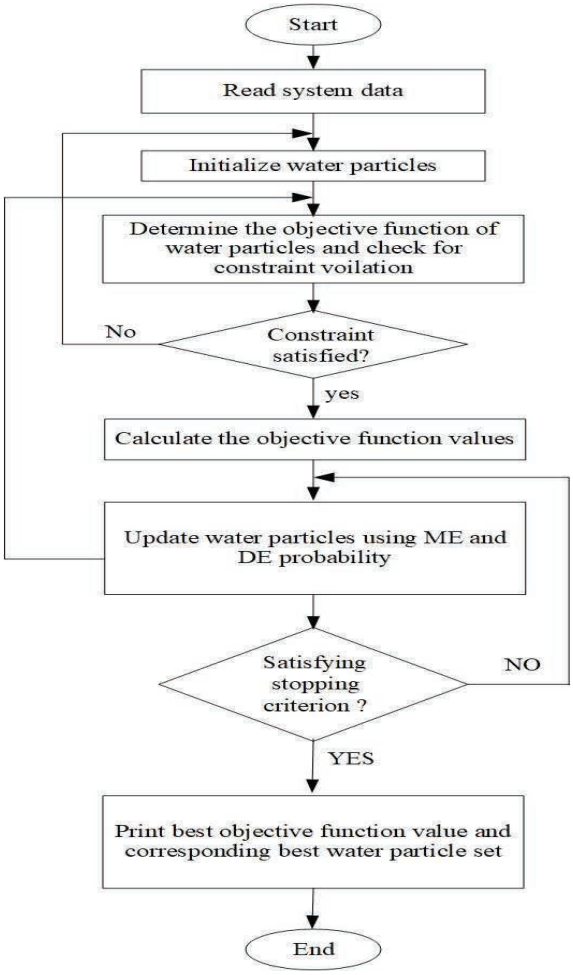

Figure 5 Flowchart of WEO.

5.2 Grey Wolf Optimization

S. Mirajalili [22] suggested a population based algorithm called grey wolf optimization (GWO). Grey wolves have a well-defined social hierarchy. The leaders are referred to as alphas. The alpha is responsible for decision making regarding the time to sleep, time to wake up, to hunt and so on. Beta is the second rank in the grey wolf pyramid. For the pack duties particularly the decision making process, the beta wolves assist the alphas. In the event that one of the alpha becomes very old or dies, the best contender to become

the alpha is generally the beta wolf. The lowest rank in the hierarchy is given to omegas. The omega wolves are used as a scapegoat, and they are forced to yield to all other main wolves at all times. These include the final count of wolves to be eaten. Any wolf excluding above ranked wolves is referred to as subordinate. Although delta wolves must bow to alphas and betas, they rule the omega. Following are the key phases of wolf hunting:

(a) The prey is being followed, pursued and advanced.
(b) Pursue the prey, encircle it and annoy it as long as it is static.
(c) Attacking the prey is a good idea.

When creating GWO, we include the most fit value as alpha (α) to quantitatively describe the social structure of wolves. As a result, the ultimate and penultimate options are known as beta (β) and delta (δ). Omega (ω) is assumed for the rest of the possible solutions and following Equations (10) and (11) are inferred.

$$\vec{Z} = |\vec{C}.\vec{Y}_P(t) - \vec{Y}(t)| \tag{10}$$

$$\vec{Y}(t+1) = \vec{Y}_P(t) - \vec{A}\vec{D} \tag{11}$$

Where, $\vec{A}$,$\vec{C}$ represent co-efficient vectors, $\vec{Y}$ indicates the grey wolf position vector, $\vec{Y}_P$ is the prey position vector and *t* indicates the current iteration. The $\vec{A}$ and $\vec{C}$ vectors are calculated using Equations (12) and (13):

$$\vec{A} = 2\vec{a}r_1 - \vec{a} \tag{12}$$

$$\vec{C} = 2\vec{r}_2 \tag{13}$$

Where, r_1, r_2 are random vectors and during the iterations process, the solutions of $\vec{a}$ are reduced progressively. To simulate the chasing performance of grey wolves mathematically, we postulate that hunting factors have superior information about prey location. As a result, the best three results are stored and other search factors are employed to update the locations in accordance with the placement of best search agent.

$$\vec{Y}_1 = \vec{Y}_\alpha - \vec{a}_1\vec{Z}_\alpha, \quad \vec{Y}_2 = \vec{Y}_\beta - \vec{a}_2\vec{Z}_\beta, \quad \vec{Y}_3 = \vec{Y}_\delta - \vec{a}_3\vec{Z}_\delta \tag{14}$$

$$\vec{Y}(t+1) = \frac{\vec{Y}_1 + \vec{Y}_2 + \vec{Y}_3}{3} \tag{15}$$

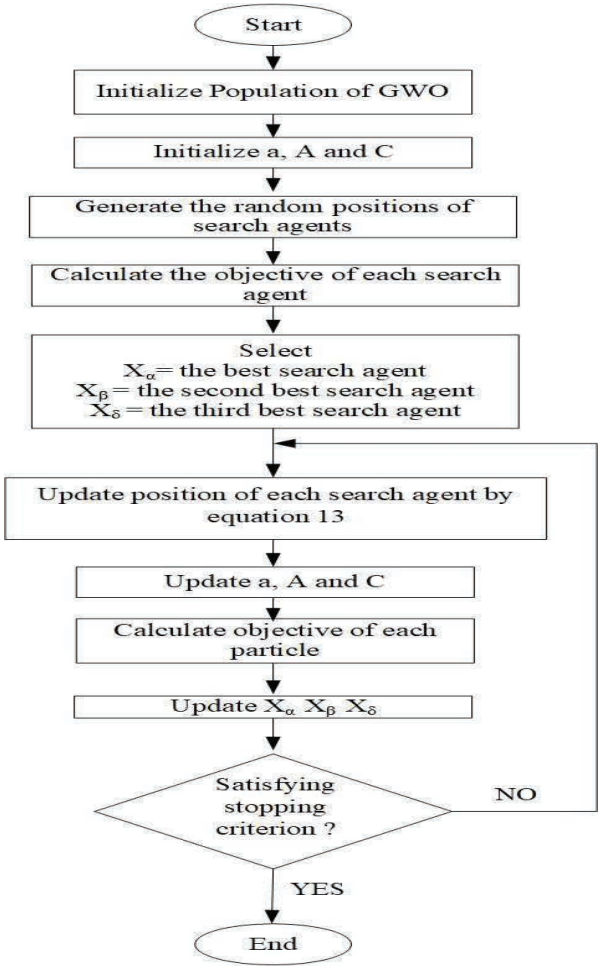

Figure 6 Flowchart of GWO.

Alpha, beta and delta determine the final position in the search space which would be a random place within a circle. The flowchart of algorithm is shown in Figure 6.

5.3 Firefly Algorithm

Flash signals are used by fireflies to attract other fireflies looking for partners. Yang created a meta-heuristic algorithm based on this phenomenon [23].

All fireflies are considered unisexual, and the intensity of their flash determines how attractive they are. As a result, if a firefly particle has to choose between two fireflies, it will be drawn to the firefly with the brightest light and will move towards that path. The firefly will move in a random path if there are no other fireflies nearby. The fitness function is linked to the brightness of the flash. As seen from Equation (16), light intensity follows the inverse square law.

$$I(r) = \frac{I_s}{r^2} \tag{16}$$

Where, I_s is the source intensity and $I(r)$ is the light intensity at a distance r.

For a static absorption co-efficient (γ) in a given medium, the light intensity (I) depends on original light intensity (I_0) and fluctuates with distance (r) as given in Equation (17).

$$I = I_0 \exp(-\gamma r^2) \tag{17}$$

Because the adherence of a firefly is related to the light ardency seen by nearby fireflies, its attractiveness (β) can be described using Equation (18):

$$\beta = \beta_0 \exp(-\gamma r^m); \quad m \geq 1 \tag{18}$$

Where, β_0 is the appealing at $r = 0$. For any two fireflies i and j at x_i and x_j respectively the distance between them is calculated in Equation (19). Each generation, the fireflies migrate to brighter fireflies nearby, as specified by Equation (20).

$$\mathrm{r}_{ij} = \sqrt{\sum_{k=1}^{d}(x_{i,k} - x_{j,k})^2} = \|x_i - x_j\| \tag{19}$$

$$x_i = x_i + \beta_0 \exp(-\gamma \mathrm{r}_{ij}^2)(x_i - x_j) + \alpha\varepsilon \tag{20}$$

Where, α denotes the parameter of randomization and ε is a random value Gaussian distribution vector. The step size is controlled by α here. Based on the brightness, the fireflies are graded at the conclusion of each iteration, which leads to the discovery of finest firefly in each iteration. In succeeding generations, the fireflies are made to travel and according to the objective function the light intensity of each firefly is streamlined. The best objective function value is determined by the firefly with the maximum brightness and

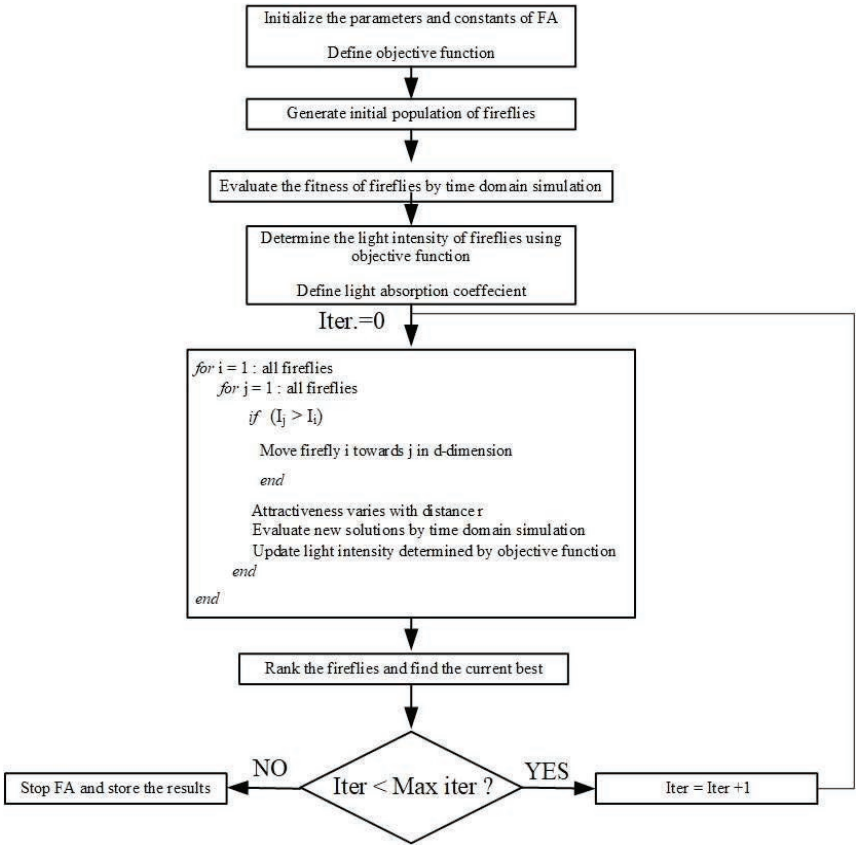

Figure 7 Flowchart of FA.

it is considered to be the best case (optimal solution) at the conclusion of all iterations. Flowchart of FA is given Figure 7.

Objective function selection for the given power system:

The location and specific value of the PID parameters is determined by the objective function. Other essential properties given in the objective function include steady state errors, settling time rise time and peak overshoot. The fitness function can be written using Equation (21):

$$F_{obj} = 1 - e^{-\delta}(M_P + E_r) + e^{-\delta}(T_s - T_r) \tag{21}$$

Where, F_{obj} represents the objective function and δ is the scaling factor.

E_r, T_s, T_r and M_P represent steady state errors, settling time rise time and peak overshoot.

6 Results and Discussions

The developed VFT model is simulated in MATLAB 2018a Simulink platform. To obtain the best results for synchronous power transfer in between connected grids a comparison based on minimization of objective function and system dynamic response regulation among the optimization techniques is done. To check the robustness of optimized PID controller gains against various changes in system parameters under nominal conditions Sensitivity analysis is performed. The investigation of power transfer is further carried to asynchronous operation of VFT.

6.1 Selection of Optimal Technique for Power System Under Nominal Conditions

The nominal system is simulated for a DC motor torque of 10 Nm, load #1 = 1 Kw, load #2 = 4 Kw, frequency = 50 Hz. The PID controller gains are optimized using GWO, WEA and FA, one at a time. The optimized PID controller gains for WEA, GWO and FA are reported in Table 1. The terms K_p, K_i, K_d represent usual controller notations while N represents the derivative coefficient of PID controller. The convergence characteristics for WEA, GWO and FA are shown in Figure 8. The obtained power transfer responses using WEA, GWO and FA techniques are compared for analysis and are shown in Figure 9. Based on the dynamic responses and objective function convergence characteristics, a comparative analysis is done for selecting the optimal technique to improve execution of the system. A critical review of Figure 9 shows that the transient characteristics of power transfer response are better handled by FA optimized PID controller. Further, the convergence of objective function (given in Equation (21)) is attained to its minimum possible value using FA technique. This analysis reflects that FA optimized PID controller achieves desired performance of the system with

Table 1 Optimized gains for PID controller using WEO, GWO and FA technique

	K_p	K_i	K_d	N
WEO	0.3182	0.4532	0.1611	0.5987
GWO	0.8717	0.9084	0.9061	5.6714
FA	0.3079	0.5157	0.3935	9.9520

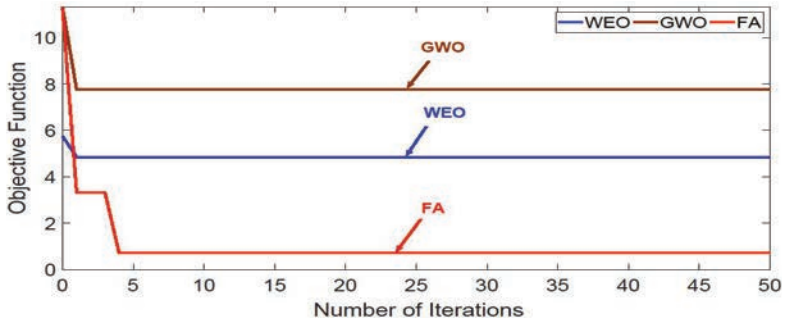

Figure 8 Convergence characteristics of WEO, GWO and FA.

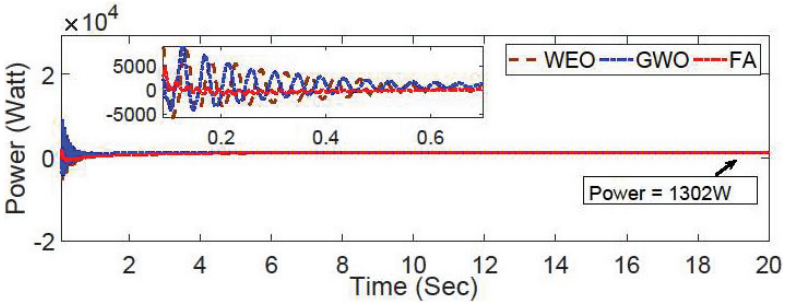

Figure 9 Power transfer using WEO, GWO and FA.

Table 2 Transient characteristics of WEO, GWO AND FA

	WEO	GWO	FA
Settling Time (seconds)	0.6 sec	0.7 sec	0.3 sec
Overshoot (% of final value)	37.09%	42.08%	25.57%
Undershoot (% of final value)	64.51%	25.19%	17.51%

minimum value of F_{obj} and better dynamic performance regulation. Thus, FA proves to be optimal technique for controller tuning for the present power system and the key specifications highlighting the superiority of FA over WEO and GWO are reported in Table 2. Further, the additional investigation is carried out with FA to be the optimal technique for performance analysis. Figure 10 shows the different values of power transfer between two grids at different values of dc motor torque. From the Figure 10, it is clear that upon increasing dc motor torque, the power transfer through VFT also increases from Grid #1 to Grid #2. Figure 11 represents the power transfer through VFT when the direction of torque is reversed. It is clear from the Figure 11

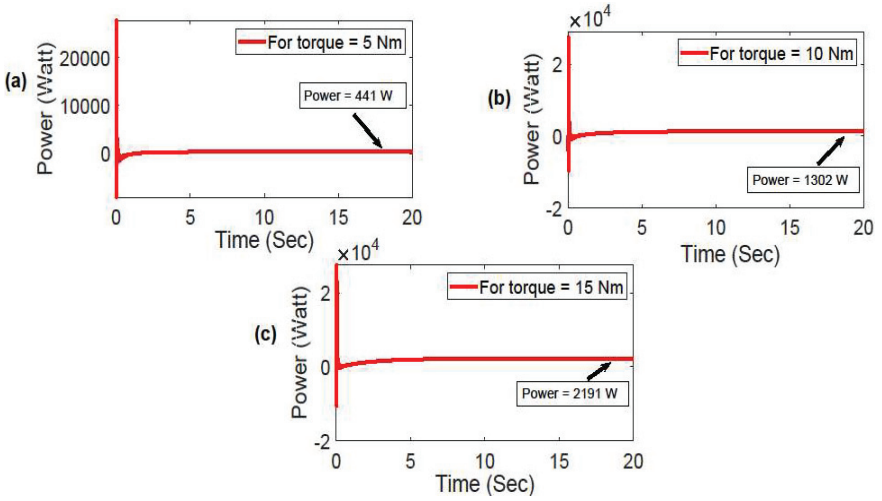

Figure 10 Power transfer for different values of positive dc motor torque using FA under synchronous condition.

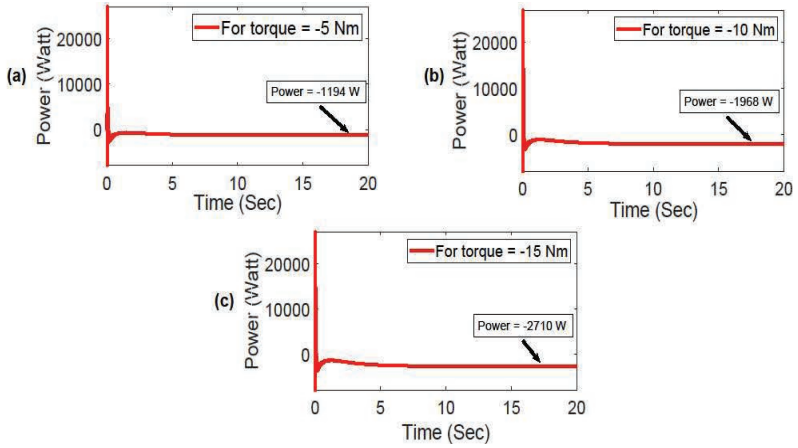

Figure 11 Power transfer for different values of negative dc motor torque using FA under synchronous condition.

that upon increasing dc motor torque in reversed direction, the power transfer also increases from Grid #2 to Grid #1. Figure 12 represents the dynamic response of VFT parameters where Figure 12(a) represents rotor current, 12(b) represents stator current, 12(c) represents dc motor torque and 12(d) represents the rotor speed in rpm. The rotor speed is zero which is due to the

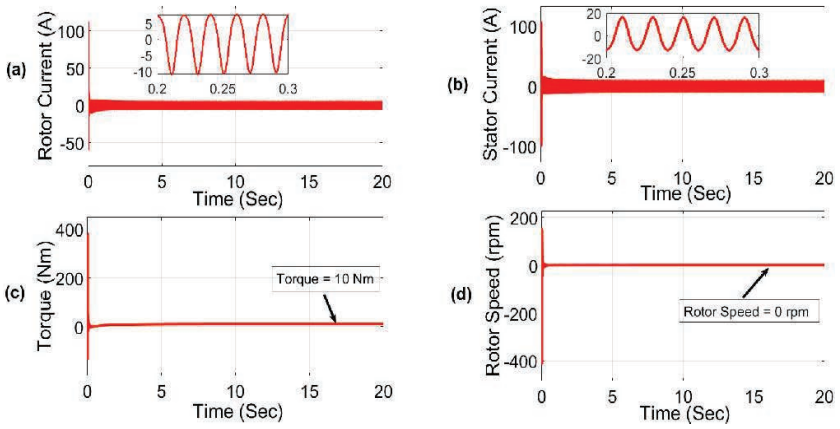

Figure 12 Dynamic response of different VFT parameters using FA under synchronous condition.

fact that both the grids are operating at same frequency. From the Figure 12 it is clear that both the rotor and stator current are sinusoidal and hence it can be deducted that VFT does not produce harmonics as compared to its other counter parts.

6.2 Sensitivity Analysis (SA)

The nominal system under any situation, may be subjected to certain disturbances which leads to instability issues [24, 25]. In order to check the behavior of the developed system to variations of system parameters, sensitivity analysis is performed with wide variations in system parameters from their nominal values. The nominal system is subjected to variations in load demand in both Grid #1 and Grid #2 and DC motor torque. The system with already FA optimized PID controller gains (Table 1) is simulated and the responses obtained under these conditions are labelled as offline-optimized responses while as the dynamic responses of the system which is once again optimized using FA technique under the changed conditions are labelled as real-time responses.

6.2.1 $\pm$10% variation in load demand in both Grid #1 and Grid #2

The developed system is altered with a load demand variation of $+10\%$ with respect to nominal load demand. The offline optimized responses are

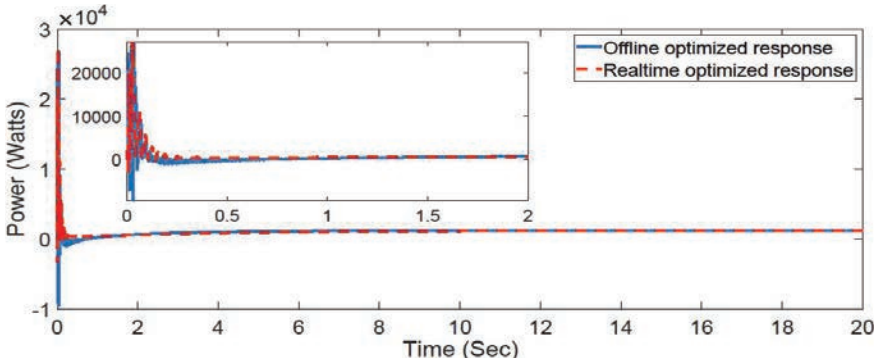

Figure 13 Comparison of real time and offline FA optimized power transfer with +10% variation in load demand.

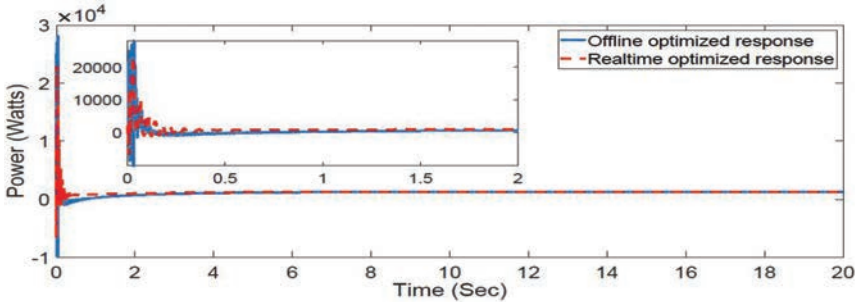

Figure 14 Comparison of real time and offline FA optimized power transfer with −10% variation in load demand.

compared with the real time responses as shown in Figure 13. Similarly, a load variation of −10% with respect to nominal load demand is done and the offline and real time responses are compared as shown in Figure 14. The dynamic comparison of the responses reveal that both offline as well as real time responses are almost identical.

6.2.2 ±10% variation of DC motor torque

The aim is to check the robustness of the PID controller gains when the torque deviates from the nominal value. The developed power system is applied with a ±10% deviation of dc motor torque and the compared responses are shown in Figures 15 and 16. The dynamic comparison of the responses in this case also reflects that the offline optimized and real time responses are almost same.

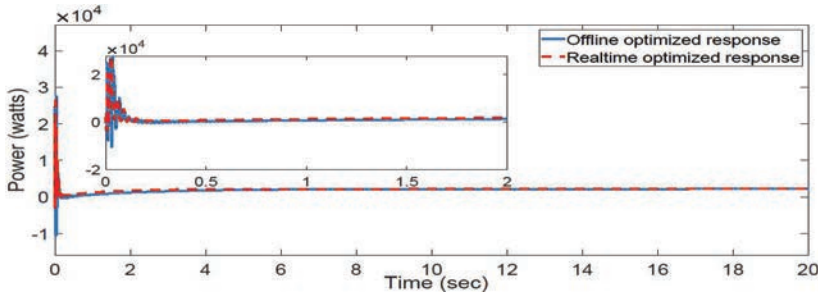

Figure 15 Comparison of real time and offline FA optimized power transfer with $+10\%$ variation in dc motor torque.

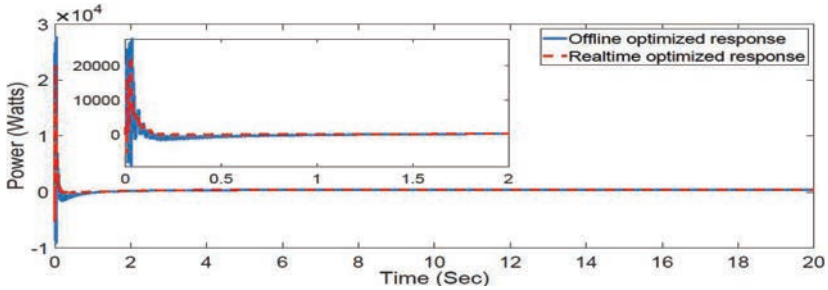

Figure 16 Comparison of real time and offline FA optimized power transfer with -10% variation in dc motor torque.

Inferences from Section 5.2: Sensitivity analysis of the system pertaining to variations from the nominal system parameters validate the effective disturbance handling capability of the optimized PID controller gains. This analysis proves that the developed power system is stable enough to withstand any change in the system parameters. Hence, the optimized PID controller gains need no further resetting.

6.3 Asynchronous Operation of the Power System

In an asynchronous interconnection, the two power grids will operate at different frequencies. The difference of frequencies between two grids makes rotor rotate continuously and speed of rotor is a function of frequency difference between rotor and stator and is given in Equation (22).

$$N_r = \left(1 - \frac{f_r}{f_s}\right) N_s \tag{22}$$

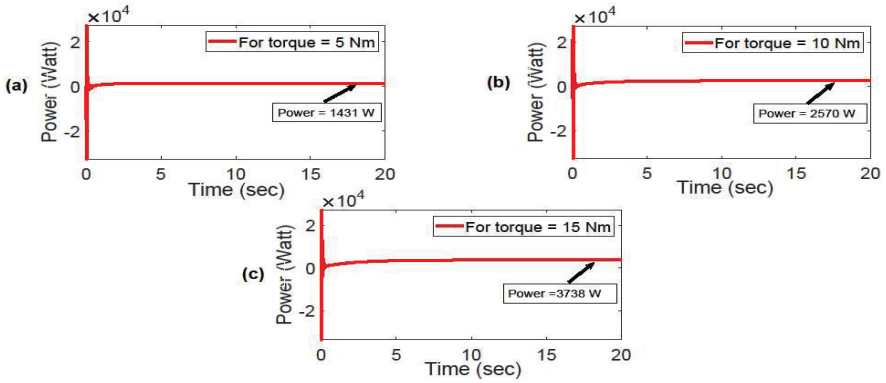

Figure 17 Power transfer for different values of positive dc motor torque using FA under asynchronous condition.

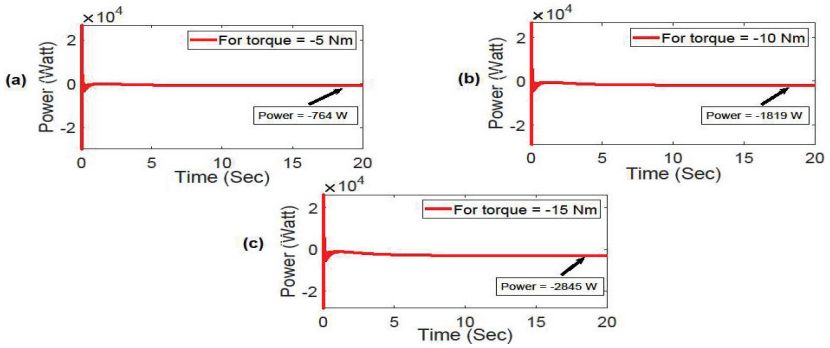

Figure 18 Power transfer for different values of negative dc motor torque using FA under asynchronous condition.

N_r = rotor speed
N_s = stator flux speed
f_s = stator frequency
f_r = rotor frequency

The rotor and stator of VFT are connected to two power grids of the present power system at different frequencies with Grid #1 operated at 60 Hz while Grid #2 is operated at 50 Hz. The system is simulated for different dc motor torque values with FA optimized PID controller gains and the simulation results are shown in Figures 17, 18 and 19. Figures 17 and 18 represents the power transfer through VFT for positive and negative values of dc motor torque respectively under asynchronous condition and it

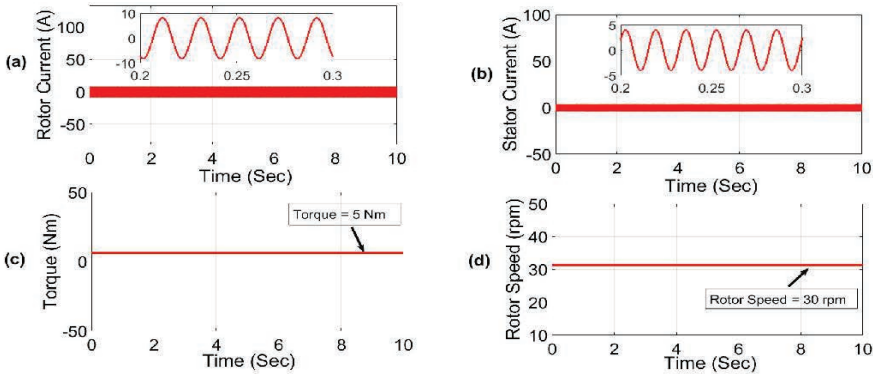

Figure 19 Dynamic response of different VFT parameters using FA under asynchronous condition.

is clear from these figures that power transfer through VFT increases upon increasing dc motor torque. Figure 19 represents the dynamic response of VFT parameters (rotor current, stator current, dc motor torque and rotor speed) under asynchronous condition and it is clear from the figure that the VFT does not produce harmonics in rotor and stator current.

6.4 Harmonic Analysis

The major phenomena that impacts the power quality is the existence of harmonics. Grid current and voltage waveforms no longer remain sinusoidal due to the operation of non-linear loads, but instead contain components at multiples of the system's fundamental frequency [26]. The non-linear converters in HVDC power transmission are replaced by VFT to suppress the harmonic content. The Total Harmonic Distortion (THD), which is the ratio of total harmonics to the value at the fundamental frequency is the most widely used indicator for characterizing the total system harmonic content [26]. To verify the harmonic content in the rotor and stator current, THD analysis has been carried out and is presented in Figures 20(a), 20(b), 21(a) and 21(b). The THD given in the Figures 20(a) and 20(b) is 1.57% and 0.79% for the rotor and stator current respectively under synchronous condition for a dc motor torque of 10 Nm. The THD given in the Figures 21(a) and 21(b) is 0.78% and 2.25% for the rotor and stator current respectively under asynchronous condition for a dc motor torque of 5 Nm. Under both the conditions the THD is completely acceptable as per standard IEEE norms [27, 28]. This validates the fact that VFT produces very less harmonics as compared to its other counter parts.

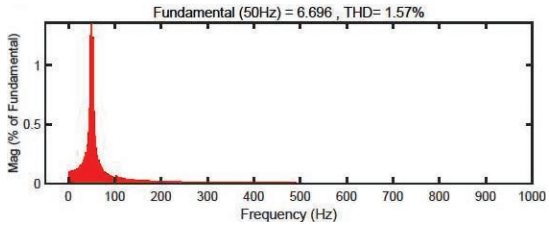

Figure 20(a) THD of rotor current under synchronous condition.

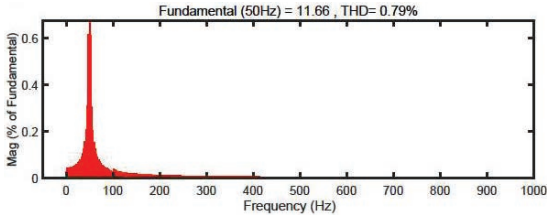

Figure 20(b) THD of stator current under synchronous condition.

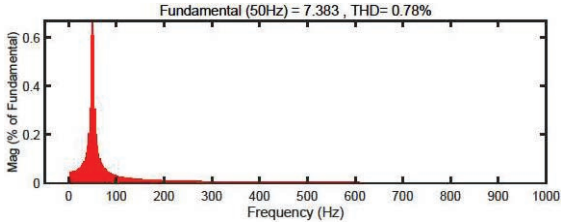

Figure 21(a) THD of rotor current under asynchronous condition.

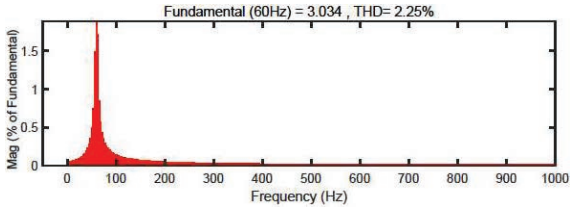

Figure 21(b) THD of stator current under asynchronous condition.

7 Conclusion

A VFT based power system employing PID controller is studied for power transfer capability interconnected between two grids. The PID controller gains are optimized using different optimization techniques where FA technique proves to be efficient enough in elevating the performance of

the power system, the performance index being better transient and steady-state characteristics and better convergence characteristics of the formulated objective function. The disturbance rejection ability of the power system is authenticated employing sensitivity analysis by deviating certain power system parameters from their nominal values. Also, the behavior of power system under asynchronous operation is studied which confers the dynamic behavior characteristics under difference in frequencies of the interconnected grids. Moreover, the THD analysis is conducted to confer the effective suppression of rotor and stator current harmonics by VFT which improves the quality of power transfer between two connected grids.

Appendix

Nominal system parameters

WRIM

Rated nominal power (S_{WRIM}): 10 Kva, voltage (V_{l-l} rms): 400 V, f: 50 Hz, rotor-resistance (R_r): 1.395 Ω, stator-resistance (R_s): 1.405 Ω, rotor-inductance (L_r): 0.005839 H, stator-inductance (L_s): 0.005839 H, mutual-inductance (L_m): 0.1722.

DC Motor

Power (P_{dc}): 1 HP, field voltage (V_f): 300 V, armature voltage (V_a): 240 V, field resistance (R_f) and inductance (L_f): 281.3 Ω and 156 H, armature resistance (R_a) and inductance (L_a): 2.581 Ω and 0.028 H.

Grid #1 and Grid #2

Voltage voltage (V_{l-l} rms): 400 V, f: 50 Hz, source resistance (R_s): 0.8929 Ω.

Optimization Technique

WEO: – Pop size = 50, E_{cs}max = −0.5, E_{cs}min = −3.5, $\phi_{max} = 50$ degree, $\phi_{min} = 20$ degree, computational time = 14 min.

GWO: - pop size = 50, $\vec{a} = [2, 0]$ linearly decreased over the course of iterations, $\vec{r_1}$ $\vec{r_2} = [0, 1]$, computational time = 17 min.

FA: – pop size = 50, $\alpha = 0.3$, $\beta_0 = 0.2$, $\gamma = 1$, computational time = 15.

Acknowledgements

The authors are grateful to the National Institute of Technology, Srinagar, for giving access to foreign publications and for allowing us to conduct research at the institute.

References

[1] Bakhsh FI, Irshad M and Asghar MSJ. Modeling and simulation of variable frequency transformer for power transfer in-between power system networks. India International Conference on Power Electronics 2010 (IICPE2010), 2011, pp. 1–7, doi: 10.1109/IICPE.2011.5728119.

[2] Ambati BB, Khadkikar V. Variable Frequency Transformer Configuration for Decoupled Active-Reactive Powers Transfer Control. *in IEEE Transactions on Energy Conversion,* vol. 31, no. 3, pp. 906–914, Sept. 2016, doi: 10.1109/TEC.2016.2550558.

[3] Merkhouf A, Doyon P, Upadhyay S. Variable Frequency Transformer—Concept and Electromagnetic Design Evaluation. *in IEEE Transactions on Energy Conversion*, vol. 23, no. 4, pp. 989–996, Dec. 2008, doi: 10.1109/TEC.2008.2001460.

[4] Truman P, Stranges N. A Direct Current Torque Motor for Application on a Variable Frequency Transformer. *2007 IEEE Power Engineering Society General Meeting, Tampa, FL, 2007*, pp. 1–5, doi: 10.1109/PES.2007.385703.

[5] Rahul R, Jain AK, Bhide R. Analysis of variable frequency transformer used in power transfer between asynchronous grids. *2012 IEEE International Conference on Power Electronics, Drives and Energy Systems (PEDES), Bengaluru,* 2012, pp. 1–5, doi: 10.1109/PEDES.2012.6484423.

[6] Bagen B, Jacobson D, Lane G, Turanli HM. Evaluation of the Performance of B2B HVDC Converter and Variable Frequency Transformer for Power Flow Control in a Weak Interconnection. *2007 IEEE Power Engineering Society General Meeting, Tampa,* FL, 2007, pp. 1–6, doi: 10.1109/PES.2007.385809.

[7] Bakhsh FI, Khatod DK, Malik H. Fault Analysis of Variable Frequency Transformer (VFT) for Power Transfer in-between Synchronous Grids. Soft Computing in Condition Monitoring and Diagnostics of Electrical

and Mechanical Systems, Advances in Intelligent Systems and Computing, pp. 269–286, Springer Nature, Singapore, January 2020. doi: 10.1007/978-981-15-1532-3_12.

[8] S. Chen, J. Lu, G. Zhang and Y. Zhang, "Immunizing Variable Frequency Transformer From Dual-Side Asymmetrical Grid Faults via a Single-Converter-Based Novel Control Strategy," *in IEEE Transactions on Power Delivery,* vol. 35, no. 3, pp. 1330–1338, June 2020, doi: 10.1109/TPWRD.2019.2940771.

[9] Bakhsh FI, Khatod DK. Application of variable frequency transformer (VFT) for grid interconnection of PMSG based wind energy generation system. *Sustainable Energy Technologies and Assessments*, Volume 8, 2014, Pages 172–180, doi: 10.1016/j.seta.2014.09.003.

[10] Bakhsh FI, Khatod DK. A new synchronous generator based wind energy conversion system feeding an isolated load through variable frequency transformer. *Renewable Energy,* Volume 86, 2016, Pages 106–116, doi: 10.1016/j.renene.2015.07.093.

[11] Wang L, Chen L. Reduction of Power Fluctuations of a Large-Scale Grid-Connected Offshore Wind Farm Using a Variable Frequency Transformer. *in IEEE Transactions on Sustainable Energy*, vol. 2, no. 3, pp. 226–234, July 2011, doi: 10.1109/TSTE.2011.2142406.

[12] Chellaswamy C, Muthammal R, Kumar NP, Ramesh R. Reduction of Power Fluctuation in Wind Turbine Using Variable Frequency Transformer and Optimized PID Controller. *in Asian Journal of Applied Science*, Vol. 5, no. 5, Oct 2017, pp. 868–877, doi: 10.24203/ajas.v5 i5.5037.

[13] Guha D, Roy PK, Banerjee S. Load frequency control of interconnected power system using grey wolf optimization. *Swarm and Evolutionary Computation*, Volume 27, 2016, Pages 97–115, ISSN 2210-6502, https: //doi.org/10.1016/j.swevo.2015.10.004.

[14] Shakarami MR, Davoudkhani IF. Wide-area power system stabilizer design based on Grey Wolf Optimization algorithm considering the time delay. *Electric Power Systems Research*, Volume 133, 2016, Pages 149–159, ISSN 0378-7796, doi.org/10.1016/j.epsr.2015.12.019.

[15] Saha A, Bhattacharya A, Das P, Chakraborty AK. Water evaporation optimization technique for static optimal power flow problems. *in 2nd IEEE International Conference for Convergence in Technology (I2CT)*, April, 2017.

[16] Saha A, Das P, Chakraborty AK. Water evaporation algorithm: A new metaheuristic algorithm towards the solution of optimal power flow.

International Journal of Computational Engineering Science, https://doi.org/10.1016/j.jestch.2017.12.009.

[17] Sekhar GTC, Sahu RK, Baliarsingh AK, Panda S. Load frequency control of power system under deregulated environment using optimal firefly algorithm. *International Journal of Electrical Power & Energy Systems*, Volume 74, 2016, Pages 195–211, ISSN 0142-0615, https://doi.org/10.1016/j.ijepes.2015.07.025.

[18] Balachennaiah P, Suryakalavathi M, Nagendra P. Firefly algorithm based solution to minimize the real power loss in a power system. *Ain Shams Engineering Journal*, Volume 9, Issue 1, 2018, Pages 89–100, ISSN 2090-4479, https://doi.org/10.1016/j.asej.2015.10.005.

[19] Manzoor S, Bakhsh FI, Mufti M. Coordinated control of VFT and fuzzy based FESS for frequency stabilisation of wind penetrated multi-area power system. Wind Engineering. July 2021. doi: 10.1177/0309524X21 1030846.

[20] Manzoor S, Mufti M, Bakhsh F I. Application of VFT coordinated with fuzzy based SCESS for load frequency control. International Journal of Power and Energy Systems, Vol. 41, No. 4, June 2021.

[21] Kaveh A, Bakhshpoori T. Water Evaporation Optimization: A novel physically inspired optimization algorithm. *Computers & Structures*, Volume 167, 2016, Pages 69–85, ISSN 0045-7949, https://doi.org/10 .1016/j.compstruc.2016.01.008.

[22] Mirjalili S, Mirjalili SM, Lewis A. Grey Wolf Optimizer. *Advances in Engineering Software*, Volume 69, 2014, Pages 46–61, ISSN 09659978 https://doi.org/10.1016/j.advengsoft.2013.12.007.

[23] Yang XS. Firefly Algorithms for Multimodal Optimization. in *Watanabe O., Zeugmann T. (eds) Stochastic Algorithms: Foundations and Applications. SAGA 2009*, lecture Notes in Computer Science, vol. 5792. Springer, Berlin, Heidelberg. https://doi.org/10.1007/978-3-642-04 944-6_14.

[24] Farooq Z, Rahman A, Lone SA. System dynamics and control of EV incorporated deregulated power system using MBO-optimized cascaded ID-PD controller. *International Transactions on Electrical Energy Systems*. 2021 Nov;31(11):e13100.

[25] Safiullah S, Rahman A, Ahmad Lone S. Optimal control of electrical vehicle incorporated hybrid power system with second order fractional-active disturbance rejection controller. *Optim Control Appl Meth.* 2021; 1–30.

[26] J. Guo, J. Yang, P. Ivry and C. Serrano, "Analysis of the Impacts of V2G Chargers on LV Grid Harmonics," *2020 9th International Conference on Renewable Energy Research and Application (ICRERA), 2020*, pp. 88–92, doi: 10.1109/ICRERA49962.2020.9242787.
[27] British Standards Institute, "*IEC 61000-3-2*: 2014 Electromagnetic compatibility (EMC)-Part3-2: Limits for harmonic current emissions (equipment input current $\leq$ 16A per phase)," 2014.
[28] The Institute of Electrical and Electronics Engineers, "*IEEE 519*: IEEE recommended practice and requirements for harmonic control in electric power systems," 2014.

Biographies

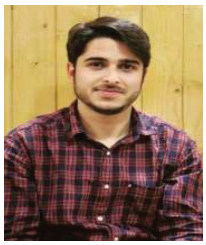

Aabid Hussain Sheikh, born in jammu and kashmir in april 1991, graduated in Electrical Engineering from Jammu University in 2013 and received his Master's in Power Systems from Al-falah university in 2017. He is currently pursuing Ph.D from National institute of technology, srinagar, jammu and kashmir. His areas of interest include variable frequency transformer, optimization techniques, power electronics and drives and power systems.

Farhad Ilahi Bakhsh received Diploma and B. Tech degree in Electrical Engineering from Aligarh Muslim University (AMU), Aligarh, India in 2006

and 2010, respectively. He was awarded University Medal (Gold) for standing first throughout Diploma In Electrical Engineering. Then he pursued Masters in Power System and Drives from the same University. In Masters he secured first position in his branch. He joined IEEE during Masters and since then he is an IEEE member. He also worked as head of Research & Development cell, IEEE student chapter, AMU for around two years. Under this cell, he developed five new systems i.e. A rotor power control based flexible asynchronous AC link (FASAL) system, A miss-call based switching system for multiple loads or appliances, A power controller circuit based flexible asynchronous AC link (FASAL) system for induction generator applications, A combined voltage control and rotor power control based flexible asynchronous AC link (FASAL) system and A waste fluid pressure based energy generation system. Among these five systems, four system has been published by an official Journal of Patent Office.

Then he pursued Ph.D. from Indian Institute of Technology Roorkee, India. During his Ph.D. he developed a new method for grid integration for wind energy generation system which has been recognized worldwide. He served as Assistant Professor in Department of Electrical & Renewable Energy Engineering, School of Engineering & Technology, Baba Ghulam Shah Badshah University, Rajouri, J & K, India. He developed an automatic solar tracking system which has been appreciated by IEEE India Council, Centre for Embedded Product Design, Centre for Electronics Design and Technology, Netaji Subhas Institute of Technology in association with IEEE Delhi Section & IEEE CAS, Bangalore Chapter. Currently he is serving as Assistant Professor in Department of Electrical Engineering, National Institute of Technology Srinagar, Jammu & Kashmir, India. He is founder and Counselor of IEEE Student Branch, NIT Srinagar.

Recently, he has won "10 for 10 Typhoon HIL Award" from Switzerland, Europe. He delivered a number of Keynote talks, Invited talks and Expert Lectures at National and International level in conferences, workshops, STC, etc. He has more than 50 published papers in International reputed Journals, International and National reputed Conferences. Many times, he got best paper awards in International conferences. Moreover, he has Indian and Australian granted patents in his credit. He is the Associate Editor of Distributed Generation & Alternative Energy Journal and Guest Editor in IET Generation, Transmission and Distribution Journal. His research area of interests includes Performance Analysis of Variable Frequency Transformer, Application of Power Electronics in Renewable Energy Systems (Solar & Wind), Multilevel Converters, Multi-phase Drives and Alternate Energy Vehicles.